Inorganic Chemistry

Article

pubs.acs.org/IC

Ligand Exchange and Spin State Equilibria of Fe^{II}(N4Py) and Related Complexes in Aqueous Media

Apparao Draksharapu,[†] Qian Li,[†] Hella Logtenberg,[†] Tieme A. van den Berg,[†] Auke Meetsma,[‡] J. Scott Killeen,[§] Ben L. Feringa,[†,‡] Ronald Hage,[∥] Gerard Roelfes,[†,‡] and Wesley R. Browne*[,†,‡]

[†]Stratingh Institute for Chemistry, Faculty of Mathematics and Natural Sciences, University of Groningen, Nijenborgh 4, 9747AG Groningen, The Netherlands

[‡]Zernike Institute for Advanced Materials, Faculty of Mathematics and Natural Sciences, University of Groningen, Nijenborgh 4, 9747AG Groningen, The Netherlands

[§]Unilever R&D Vlaardingen, P.O. Box 114, 3130 AC Vlaardingen, The Netherlands

[∥]Rahu Catalytics BV, BioPartner Center Leiden, Wassenaarseweg 72, 2333, AL Leiden, The Netherlands

Supporting Information

ABSTRACT: We report the characterization and solution chemistry of a series of Fe^{II} complexes based on the pentadentate ligands N4Py (1,1-di(pyridin-2-yl)-*N*,*N*-bis(pyridin-2-ylmethyl)methanamine), MeN4Py (1,1-di(pyridin-2-yl)-*N*,*N*-bis(pyridin-2-ylmethyl)ethanamine), and the tetradentate ligand Bn-N3Py (*N*-benzyl-1,1-di(pyridin-2-yl)-*N*-(pyridin-2-ylmethyl)methanamine) ligands, i.e., $[Fe(N4Py)(CH_3CN)](ClO_4)_2$ (**1**), $[Fe(MeN4Py)(CH_3CN)](ClO_4)_2$ (**2**), and $[Fe(Bn\text{-}N3Py)(CH_3CN)_2](ClO_4)_2$ (**3**), respectively. Complexes **2** and **3** are characterized by X-ray crystallography, which indicates that they are low-spin Fe^{II} complexes in the solid state. The solution properties of **1**−**3** are investigated using ^{1}H NMR, UV/vis absorption, and resonance Raman spectroscopies, cyclic voltammetry, and ESI-MS. These data confirm that in acetonitrile the complexes retain their solid-state structure, but in water immediate ligand exchange of the CH_3CN ligand(s) for hydroxide or aqua ligands occurs with full dissociation of the polypyridyl ligand at low (<3) and high (>9) pH. pH jumping experiments confirm that over at least several minutes the ligand dissociation observed is fully reversible for complexes **1** and **2**. In the pH range between 5 and 8, complexes **1** and **2** show an equilibrium between two different species. Furthermore, the aquated complexes show a spin equilibrium between low- and high-spin states with the equilibrium favoring the high-spin state for **1** but favoring the low-spin state for **2**. Complex **3** forms only one species over the pH range 4−8, outside of which ligand dissociation occurs. The speciation analysis and the observation of an equilibrium between spin states in aqueous solution is proposed to be the origin of the effectiveness of complex **1** in cleaving DNA in water with $^3O_2$ as terminal oxidant.

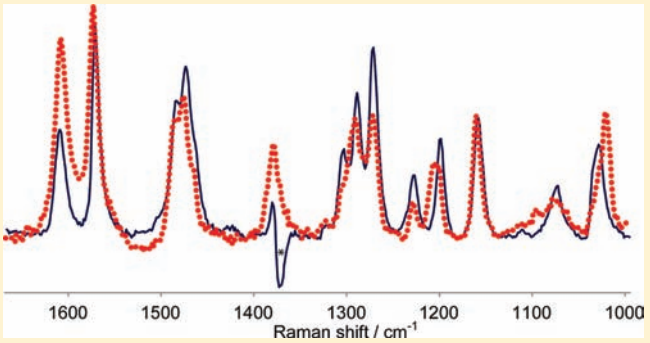

INTRODUCTION

Bleomycins (BLMs) are a class of glycopeptide antibiotics isolated from *Streptomyces verticillus* and are used in the clinical treatment of head, neck, and testicular cancers.[1] The iron complex of bleomycin (Fe-BLM) is capable of effecting efficient cleavage of DNA[1,2] and catalyzes oxidation of a number of organic substrates with $^3O_2$ or H_2O_2,[3] respectively. The mechanism by which $^3O_2$ is activated by nonheme iron systems, such as Fe-BLM, has received much attention recently.[4] Many structural and functional model complexes for metallobleomycins have been developed in particular as synthetic DNA cleaving agents.[5,6] Our group, together with Que and coworkers, has developed the pentadentate ligand 1,1-di(pyridin-2-yl)-*N*,*N*-bis(pyridin-2-ylmethyl)methanamine) (N4Py) as a structural and functional model for the metal binding domain of the BLM.[7,8] The Fe^{II} complex $[Fe^{II}(N4Py)(CH_3CN)](ClO_4)_2$ (**1**) has been characterized and shown to be active both in organic functional group oxidative transformations with various terminal oxidants[9] and in the oxidative cleavage of DNA with $^3O_2$.[7b,10] To date, mechanistic studies of complex **1** and related complexes have focused either on their chemistry and catalytic activity in nonaqueous solvents, where the terminal oxidant employed is H_2O_2,[7a,9] peracids,[11] or iodosylbenzenes,[12] or on the cleavage of DNA in water with $^3O_2$.[10] The activity of **1** in generating the active oxidant species with $^3O_2$ that are capable of achieving DNA cleavage is remarkable,[7b,10,13] and the reaction of **1** with $^3O_2$ is proposed to lead ultimately to formation of a low-spin Fe^{III}−OOH species.[7c,14] The Fe^{III}−OOH species is considered to be the precursor for the active species that is

Received: August 27, 2011
Published: December 23, 2011

responsible for DNA cleavage.[10c] It is apparent that the first step in the catalytic cycle is the oxidation of Fe^{II} to Fe^{III} by $^3O_2$ to form superoxide either by inner or outer sphere electron transfer.[15] Recently we have shown that the DNA cleaving activity of **1** can be enhanced further by excitation with light (between 350 and 480 nm) in which excitation into the ^{1}MLCT absorption bands of **1** leads to a rate enhancement for DNA cleavage.[13] The enhancement is possibly due to the removal of the spin forbidden nature of the electron transfer reaction between **1** and $^3O_2$ or by transient partial ligand dissociation.

To understand the oxidation activity of Fe^{II}(N4Py) complexes in water with $^3O_2$ as terminal oxidant it is essential to understand the species formed from **1** when dissolved in water, as it is these species which react with $^3O_2$. In this contribution, we report a combined electrochemical and spectroscopic study of **1** in aqueous and nonaqueous media. The goal is to understand the effect of redox state and pH on the coordination chemistry and electronic properties of **1** in solution. It is shown that in water **1** exhibits a remarkable pH dependence in its electrochemical and spectroscopic properties, whereas in acetonitrile **1** is stable and retains the molecular structure it has in the solid state. It is demonstrated that there are several pH-dependent equilibria, involving acid/base chemistry, ligand dissociation, interchange between penta- and tetra-denticity of the N4Py ligand and importantly equilibria between spin states of the species that are present at near neutral pH values. The latter equilibria between singlet and (presumably an intermediate) triplet and quintet states may hold the key to understanding why **1** interacts with $^3O_2$ to ultimately cleave DNA and the enhancements in the DNA cleavage activity of **1** observed upon irradiation with UV and visible light.[13]

The complexes $[Fe(MeN4Py)(CH_3CN)](ClO_4)_2$ (**2**) (MeN4Py = 1,1-di(pyridin-2-yl)-*N*,*N*-bis(pyridin-2-ylmethyl)-ethanamine) and $[Fe(Bn\text{-}N3Py)(CH_3CN)_2](ClO_4)_2$ (**3**) (Bn-N3Py = *N*-benzyl-1,1-di(pyridin-2-yl)-*N*-(pyridin-2-ylmethyl)-methanamine), which are structurally analogous to **1**, are investigated also (Figure 1) and their properties are compared

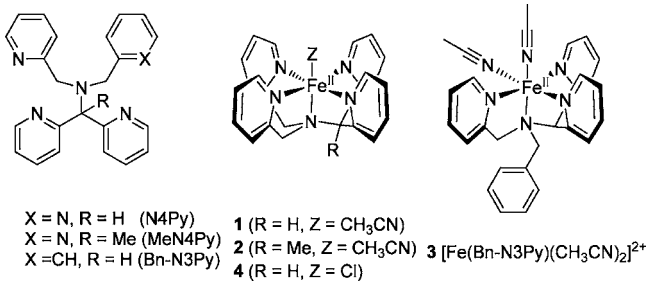

Figure 1. Structure of the ligands N4Py, MeN4Py, and Bn-N3Py, and their iron complexes **1**−**4**.

and contrasted with those of **1**. In complex **2**, the N4Py ligand is modified with a methyl group at the tertiary carbon of the ligand (MeN4Py). In complex **3**, one of the pyridine rings is replaced by a phenyl ring (Bn-N3Py) to increase the number of coordination sites available for solvent on the complex and to estimate the effect of partial ligand dissociation on the spectroscopic and electrochemical properties of **1**.

EXPERIMENTAL SECTION

Synthesis. The ligands 1,1-di(pyridin-2-yl)-*N*,*N*-bis(pyridin-2-ylmethyl)methanamine (N4Py)[7a] and *N*-benzyl-*N*-[di(2-pyridinyl)-methyl]-*N*-(2-pyridinylmethyl)amine (Bn-N3Py)[16] were prepared by literature methods. The complexes $[Fe(N4Py)(CH_3CN)](ClO_4)_2$ (**1**),[8] $[(Bn\text{-}N3Py)Fe(CH_3CN)_2](ClO_4)_2$ (**3**),[16] and $[Fe(N4Py)(Cl)](ClO_4)$ (**4**)[8] were prepared and isolated as previously reported. The synthesis and characterization of d_5-N4Py, d_5-**1**, MeN4Py (1,1-di(pyridin-2-yl)-*N*,*N*-bis(pyridin-2-ylmethyl)ethanamine), and **2** are available in the Supporting Information. Commercially available chemicals were used without further purification unless stated otherwise. Solvents for electrochemical and spectroscopic measurements were UVASOL (Merck) grade or better. In addition to using well characterized isolated complexes, for comparison in situ preparation of complexes in argon-purged double-distilled water was carried out by dissolving $FeSO_4{\cdot}7H_2O$ with one equivalent of the ligand, followed by adjustment of the pH with H_2SO_4 or NaOH to pH 6.

Caution! *Perchlorate salts of metal complexes incorporating organic ligands are potentially explosive. These compounds should be prepared in small quantities and handled with suitable protective safeguards.*

Physical Methods. For details of FTIR and Raman spectroscopy of **1**−**3** and X-ray crystallography of complexes **2** and **3**, see the Supporting Information. ^{1}H NMR spectra (400 and 600 MHz) were recorded on a Varian Mercury Plus. Chemical shifts are denoted relative to the residual solvent peak (^{1}H NMR spectra CD_3CN, 1.94 ppm; D_2O, 4.79 ppm; CD_3Cl, 7.26 ppm). pD for ^{1}H NMR studies was controlled by addition of NaOD or H_2SO_4 (diluted in D_2O) and measured using a pH meter; pD values are not adjusted for the difference between the pD/pH scales and are therefore indicative only. Elemental analyses were performed with a Foss-Heraeus CHN Rapid or a EuroVector Euro EA elemental analyzer. UV/vis absorption spectra were recorded with a HP8453 spectrophotometer or a Specord600 (AnalytikJena) in 1-cm path length quartz cuvettes. Electrochemical measurements were carried out on a model CHI760B Electrochemical Workstation (CH Instruments). Analyte concentrations were typically 0.25−0.5 mM in water containing 10 mM potassium nitrate and in acetonitrile containing 0.1 M tetrabutylammonium hexafluorophosphate [(TBA)PF_6]. Unless stated otherwise, a 3-mm-diameter Teflon-shrouded glassy carbon working electrode (CH Instruments), a Pt wire auxiliary electrode, and an SCE or Ag/AgCl reference electrode were employed. Cyclic voltammograms were obtained at sweep rates between 1 mV s^{-1} and 1 V s^{-1}. All potential values are quoted with respect to the SCE. Redox potentials are reported ±10 mV. ESI-MS spectra of ligands were recorded on a Triple Quadrupole LC/MS/MS mass spectrometer (API 3000, Perkin-Elmer Sciex Instruments). Mass spectra in ^{t}BuOH/H_2O solvent mixtures were measured as described previously[17] in positive mode and in the range m/z 100−900. Samples were prepared using doubly distilled water and pH was adjusted using dilute aqueous H_2SO_4 and NaOH solutions. Solutions were purged with argon to exclude $^3O_2$ prior to measurements.

RESULTS

The synthesis and characterization of the complexes described in the present study were described elsewhere,[7−9] at least in part, and will be discussed here only briefly. The structure of the complexes in acetonitrile solution is confirmed by a combination of solid-state and solution Raman spectroscopy together with X-ray structural analysis. Isotope labeling allows for identification of the modes observed in the Raman spectra, which, together with resonance Raman spectroscpy, allows for vibrational characterization of complexes **1**−**3** in acetonitrile and aqueous solution at submillimolar concentrations. UV/vis absorption spectroscopy together with Raman spectroscopy and electrochemistry are used to identify the existence of equilibria between species in aqueous solution and to determine the pK_a's of several of the species detected. In addition, ^{1}H NMR spectroscopy is used to provide an indication of the average spin state of the various species in solution over the pH range 2−11.

Synthesis and Characterization of 1−3. The ligand N4Py and the complex $[Fe^{II}(N4Py)(CH_3CN)](ClO_4)_2$ (**1**)

dx.doi.org/10.1021/ic201879b | *Inorg. Chem.* 2012, 51, 900−913

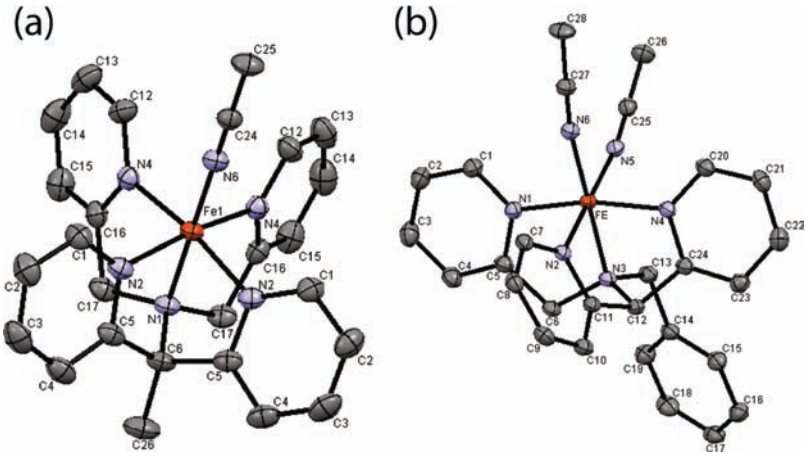

Figure 2. Structures of (a) **2** and (b) **3** with 50% probability ellipsoids.

were available from earlier studies.[7,8] d_5-N4Py, where only the alkyl hydrogen atoms are exchanged with deuterium, was prepared by heating N4Py at reflux in CH_3CO_2D.[18] The Fe^{II} complex (d_5-**1**) was prepared as for **1**. MeN4Py was prepared by deprotonation of N4Py with *tert*-butyllithium followed by methylation with methyl iodide. Complexation of MeN4Py with either $Fe(ClO_4)_3 \cdot xH_2O$ or $Fe(ClO_4)_2 \cdot 7H_2O$ in methanol/acetonitrile yielded a red crystalline complex $[Fe^{II}(MeN4Py)(CH_3CN)](ClO_4)_2$ (**2**), which was characterized by ^1H NMR spectroscopy (Figure S6) and single-crystal X-ray analysis (Figure 2). Alkylation of N3Py with benzyl chloride in the presence of K_2CO_3 provided the ligand Bn-N3Py. Complexation of Bn-N3Py with $Fe(ClO_4)_2 \cdot 7H_2O$ in methanol/acetonitrile resulted in the formation of red crystals, characterized as $[Fe^{II}(Bn\text{-}N3Py)(CH_3CN)_2](ClO_4)_2$ by Raman spectroscopy (Figure S1) and X-ray analysis (Figure 2).

Single-Crystal X-ray Structural Analysis. The crystal structure of **1** has been reported previously.[8] The crystal structures of **2** and **3** are shown in Figure 2 and the Fe−N bond lengths are compared in Table 1. The cation of **2** is located on a crystallographic mirror plane and shows a six coordinate Fe^{II} center in a slightly distorted octahedral geometry (Figure 2). Five coordination sites are occupied by N atoms from the ligand and the sixth is occupied by a molecule of acetonitrile. The five Fe−N bonds between the ligand MeN4Py and the Fe^{II} center range from 1.951(3) to 1.963(3) Å and are characteristic of low-spin Fe^{II} complexes[19] such as **1**,[8] $[Fe(bpy)_3]^{2+}$,[20] and $[Fe(TPA)(CH_3CN)_2]^{2+}$.[21]

Table 1. Fe−N Bond Lengths for Complexes 1−3

	1[8]	**2**	**3**
$Fe-N_{amine}$ (Å)	1.961 (3)	1.963 (3)	2.0121 (16)
$Fe-N_{py}$ (Å)[a]	1.967 (3)	1.951 (3)	1.9604 (15)
	1.976 (3)	1.951 (3)	1.9616 (14)
$Fe-N_{py}$ (Å)[b]	1.975 (3)	1.963 (3)	1.9616 (14)
	1.968 (3)	1.963 (3)	
$Fe-N_{acn}$ (Å)	1.915 (3)	1.927 (3)	1.9387 (17)
			1.9533 (16)
Fe-mean eq. plane (Å)	0.2071(5) Å	0.2058 (6) Å	

[a]Pyridine attached to tertiary carbon. [b]Pyridine attached to secondary carbon.

Introduction of a methyl group on the tertiary carbon of the N4Py ligand was found to have a (minor) effect on the Fe−N bond distances in **2**, with Fe−N2 bond becoming shorter than the Fe−N4 bond. The steric hindrance introduced by the methyl group results in a decrease the Fe−N bond length to the two pyridine rings attached to the tertiary carbon. The iron ion in **2** lies 0.2058(6) Å above the plane formed by the pyridine nitrogen atoms, which is less than the iron ion in **1** (0.2071(5) Å)[8] and reflects the increased stability of the complex upon introducing the methyl group. It is accompanied by elongation of the $Fe-N_{acn}$ bond (Table 1).

In the case of the cation of **3** the six-coordinate Fe^{II} center is in a distorted octahedral environment (Figure 2), ligated by four N atoms of the ligand and two from CH_3CN molecules, and arranged cis to each other. The Fe−N ligand distances range from 1.9387(17) Å for Fe1−N6 to 2.0121(16) Å for Fe1−N3. The $Fe-N_{amine}$ bond of **3** {2.0121(16)} is longer than the $Fe-N_{amine}$ bond {1.961(3)} of **1**,[8] however, overall, the Fe−N bond lengths are comparable to those found for other low-spin iron(II) complexes.[19−21] The $Fe-N_{acn}$ bond length increased slightly compared to **1** and **2**.

^1H NMR Spectroscopy. As expected for a low-spin iron(II) complex, in acetonitrile-d_3, **1**, its isotopologue d_5-**1**, **2**, and **3** are EPR silent and exhibit ^1H NMR spectra between 0 and 10 ppm (Figure S6). In the case of **3** some broadening and shifting of the signals in the ^1H NMR spectrum is observed due to exchange of the CH_3CN ligands with trace water (Figure S7).

The ^1H NMR spectra of **1** (Figure 3) in D_2O was essentially identical to that obtained by in situ formation of the complex

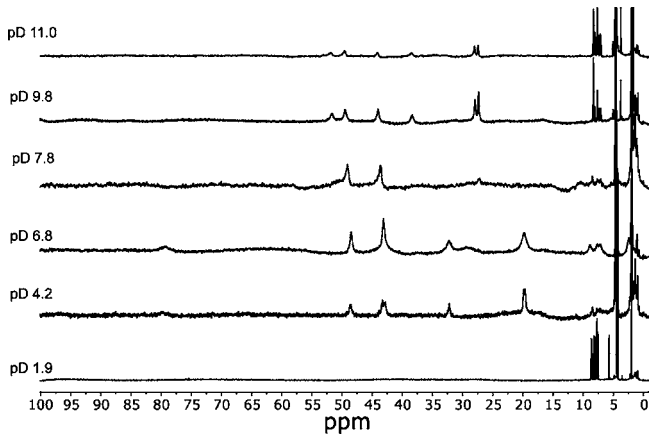

Figure 3. ^1H NMR (600 MHz) spectra of **1** in D_2O at various pD values.

dx.doi.org/10.1021/ic201879b | *Inorg. Chem.* 2012, 51, 900−913

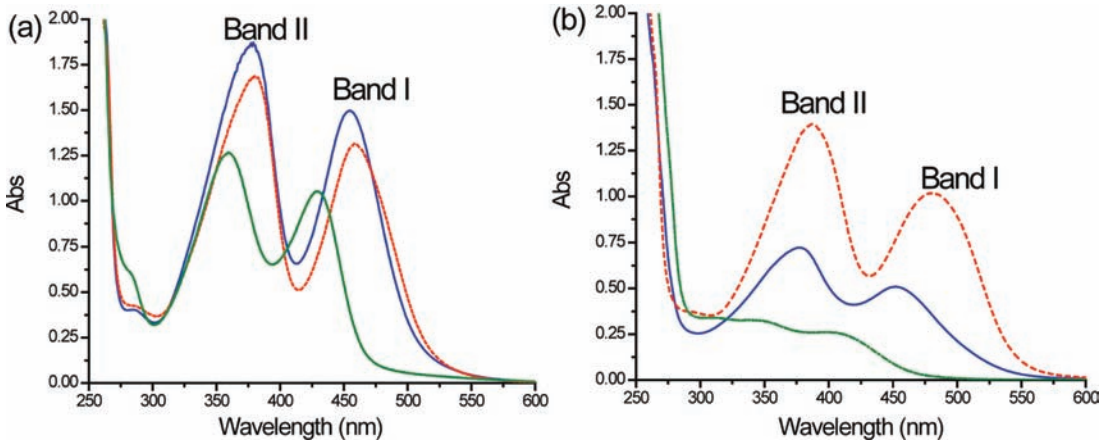

Figure 4. UV/vis absorption spectra of **1** (blue solid), **2** (red dashed) and **3** (green dashdot) in (a) acetonitrile and (b) water (at pH 6.5); all solutions are 0.25 mM.

from N4Py and $FeSO_4$ in D_2O and similar to related in situ prepared complexes,[10a,22] indicating dissociation of the CH_3CN ligand in agreement with UV/vis spectroscopy (*vide infra*). Addition of acetonitrile to **1** in D_2O results in a diamagnetic spectrum similar to that observed in acetonitrile-d_3 (Figure S11). The ^1H NMR spectra of **1** in D_2O were recorded between pD 1.9 and pD 11 (Figure 3). A considerable pD dependence is observed with broadened bands observed between 5 and 100 ppm above pD 4.2. The shift in the bands to outside of the 0−10 ppm region is due to the paramagnetic character of the species formed from **1** in water. Additionally, sharp bands were observed between 0 and 10 ppm below pD 4 and above pD 9, consistent with free ligand (Figure S8). Notably there are two distinct sets of paramagnetically shifted signals. One set is observed at pD 4.2 while the second set is observed at pD 9.8 suggesting that the two complexes are in equilibrium. pH jumping experiments confirm this (Figures S36 and S37). Between pD 6.8 and 9.8 both sets of signals are present with increased broadening observed.

The ^1H NMR spectrum of **2** in D_2O (Figure S10) shows moderate broadening compared to the spectrum of **1**, and below pD 6.5 it is otherwise similar to that observed in CD_3CN (Figure S12). Above pD 8, the appearance of weak signals of a paramagnetic complex are observed for **2** in addition to appearance of diamagnetic signals of free ligand. In contrast to **1**, ligand dissociation was not observed even at pH 1.5 indicating that the presence of the methyl substituent increases the stability of **2** considerably.

The ^1H NMR spectra of **3** were obtained between −10 and 120 ppm in D_2O over the pD range between 2 and 11 (Figure S13) and were found to be only moderately pD dependent. The spectra between pD 3 and pD 7 show relatively sharp paramagnetically shifted signals in the range 0−120 ppm. Above pD 3.8 the spectrum of a paramagnetic species is observed, while additional sharp signals are observed below pD 3.8 and above pD 8, consistent with free ligand, suggesting that ligand dissociation is more facile for **3** than for **1**. The spectra obtained at pD 3.8 and 6.5 are similar, indicating that, in contrast to **1** and **2**, for complex **3** only a single species is present in solution at intermediate pD values.

UV/vis Absorption Spectroscopy. The UV/vis absorption spectra of **1**, **2**, and **3** in acetonitrile and in water are shown in Figure 4 (see also Table S2). In acetonitrile, all three complexes show two absorption bands in the visible region assigned to metal to ligand charge transfer (^{1}MLCT) transitions (*vide infra*)[23] and pyridyl centered $\pi\rightarrow\pi^*$ transitions between 200 and 300 nm (assigned by comparison with the absorption spectrum of the free ligands). The spectra of **1** and **2** are similar apart from a small red shift in two ^{1}MLCT bands to ca. 380 and 460 nm for **2**. For compound **3** a substantial blue shift of both bands and decrease in molar absorptivity is observed, consistent with the replacement of one pyridine by a CH_3CN ligand.

The UV/vis absorption spectrum of **1** in aqueous solution (pH 6.5) is similar to that observed in acetonitrile, however a broadening of the ligand $\pi\rightarrow\pi^*$ transitions and the two absorption bands in the visible region is observed (Figure 4 and Table S2). Furthermore the visible absorption bands are half the molar absorptivity found in acetonitrile. Comparison of the UV/vis absorption spectra of **1** and **4** (where a chlorido ligand is present instead of CH_3CN) in water (pH 6.5, Figure S16) with the spectrum obtained by in situ formation of the complex from a 1:1 mixture $FeSO_4$ and the N4Py ligand confirms that, in aqueous media, the CH_3CN ligand of **1** and the chlorido ligand of **4** dissociate fully upon dissolution.[24]

For **2** both of the ^{1}MLCT absorption bands are slightly broadened in water compared to acetonitrile and are shifted to longer wavelengths (Figure 4). The molar absorptivities of the MLCT absorption bands are decreased by ca. 20% on going from acetonitrile to water. In contrast, for **3** a blue shift and broadening in the visible absorption bands as well as a substantial decrease in molar absorptivity is observed in water compared with acetonitrile (Figure 4). A near complete decrease in the absorptivity of the MLCT bands in water is expected[25] for complexes that are completely in a nonsinglet (high spin) ground state. Hence the <50% decrease for **1** and **2** indicates that there is a spin equilibrium between singlet and, e.g., quintet states in water at pH 6.5.

The broadening of the bands and the decrease in intensity is almost fully reversed by addition of 1 vol% of acetonitrile to the aqueous solution of **1** or **2** (Figure 5 and Figure S14).[26] Furthermore, the $\pi\rightarrow\pi^*$ transitions (200−300 nm) revert to the same shape, as observed in acetonitrile. The effect of added acetonitrile on the spectra of **1** and **2** obtained in water confirms that the difference between the aqueous and acetonitrile spectra is not due to solvatochromic effects but instead is due to displacement of the CH_3CN ligand by H_2O. That the equilibrium favors the CH_3CN bound complex over the aquated complex is consistent with the difference in redox potentials; the oxidation potential of Fe(II)−$NCCH_3$ complex is 400−600 mV more

dx.doi.org/10.1021/ic201879b | *Inorg. Chem.* 2012, 51, 900−913

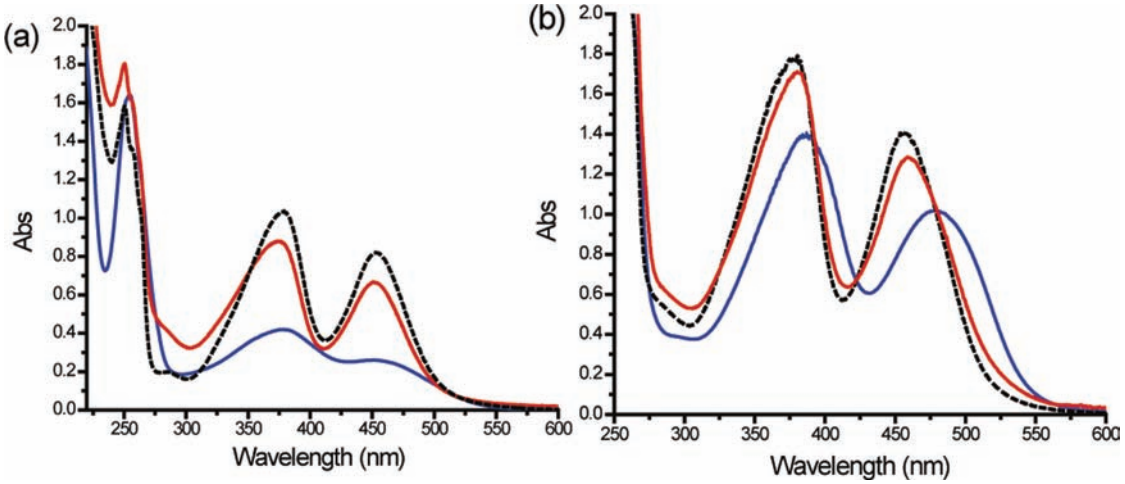

Figure 5. UV/vis absorption spectra of (a) **1** and (b) **2** in acetonitrile (black dashed), in water (pH 6, blue solid), and in water at pH 6 with 1 vol% of acetonitrile added (red dash dot).

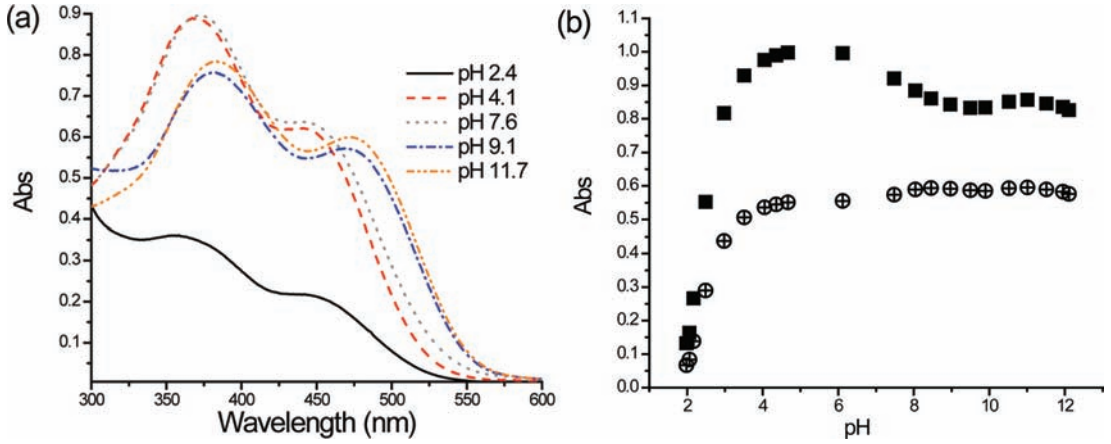

Figure 6. pH dependence of the (a) UV/vis absorption spectra and (b) absorbance at 378 (filled squares) and 454 nm (open circles) of **1** in water.

positive than that of the Fe(II)−OH_2/−OH complexes (*vide infra*). For **3**, opposite behavior is observed (Figure S15). Addition of up to 25 vol% of acetonitrile to an aqueous solution of **3** has no effect on the absorption spectrum. By contrast, addition of water to an acetonitrile solution of **3** results in a change in the spectrum to that observed in aqueous solutions when 25 vol% of water is added.

The pH dependence of the absorption spectrum of **1** in aqueous solution is shown in Figure 6. There are two distinct pH ranges over which a change in the absorption spectrum of **1** is observed. Between pH 4 and pH 2 the visible absorption bands decrease in intensity. This change is assigned to protonation of the −OH ligand on the basis of comparison with the pK_a point identified in the Pourbaix plot (*vide infra*). Between pH 6 and 8 a red shift in both absorption bands and a relatively minor decrease in intensity at 378 nm are observed for **1**.

The pH dependence of the absorption spectrum of **2** in water is shown in Figure 7a and b and contrasts sharply with that of **1**. For **2**, only a relatively minor decrease in the absorbance is observed upon lowering the pH from 6 to 1.5, which is consistent with the pK_a determined from the Pourbaix plot (*vide infra*) and with the absence of ligand peaks of the ^{1}H NMR spectra of **2** at low pH (*vide supra*). Between pH 6 and 8 a red shift in both bands and a sharp decrease in the absorbance are observed. The decrease in absorption upon an increase in pH results in **2** having a molar absorptivity similar to that of **1** at pH > 8. It should be noted that for **2** the decrease in absorption upon increase in pH is much larger than for **1** however this is due to the fact that for complex **1** at low pH the equilibrium between high- and low-spin states is more equal than for **2** which is predominantly low spin (and therefore shows more intense absorption) at below pH 7.5 (cf. NMR section and Scheme 3). The changes are fully reversible upon lowering the pH again (see Figures S36 and S37 for pH jumping experiments).

The UV/vis absorption spectra of **3** in water are pH independent between pH 4 and 7 (Figure S17a and b). Below pH 4 and above pH 8, a decrease and an increase (due to scattering as a result of the formation of a precipitate), respectively, is observed, and based on ^{1}H NMR spectroscopy (Figure S13), is assigned to ligand dissociation.

Resonance Raman spectroscopy. Resonance Raman spectroscopy has proven to be a powerful tool in the characterization of transition metal polypyridyl complexes in solution at photophysically relevant concentrations (i.e., < 1 mM).[27] Furthermore, the selective nature of the resonant enhancement of scattering from vibrational modes coupled to electronic transitions[28] allows for a deeper understanding of the nature of the absorption bands, for instance, as metal to ligand charge transfer (MLCT) transitions to specific ligand moieties. Previously resonance Raman spectroscopy has been employed to study the Fe^{III}−OOH species formed from **1** with H_2O_2.[7c,14] In the present study resonance Raman spectroscopy is

dx.doi.org/10.1021/ic201879b | *Inorg. Chem.* 2012, 51, 900−913

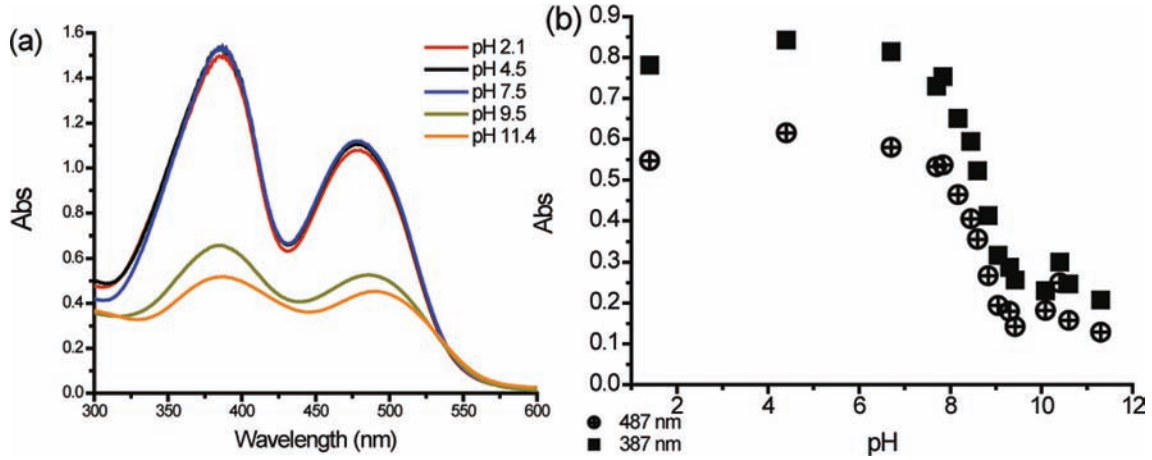

Figure 7. pH dependence of the absorption spectra of **2** in water. The decrease in absorption between pH 7.5 and 9.5 is due to a change in the structure of the complex from a predominantly low-spin state to a structure which is high-spin Fe(II) (see Scheme 3).

employed to probe the electronic origin of the visible absorption bands observed in both acetonitrile and aqueous solutions and to monitor changes in the first coordination sphere of the complexes. Importantly the vibrational modes of the ligand alkyl amine backbone are enhanced in addition to the pyridyl modes, which allow for changes in the conformation of the ligand coordinated to the Fe^{II} ion to be identified.

The solid state Raman spectra of complexes **1**, **2**, **3** and d_5-**1** are shown in Figure S1. These data confirm that the structure of complexes **1** and **2**, i.e., the pentadentate coordination of the N4Py ligand to the Fe^{II} center, is retained in acetonitrile solution (see Supporting Information for detailed discussion).

Resonance Raman Spectroscopy in Acetonitrile. Complex **1** has two absorption bands in the visible region (Figure 4). Raman spectra, recorded in optically dilute solutions (0.1 mM) in acetonitrile at λ_{exc} 355, 400.8, 449, and 473 nm, show both strong enhancements of the Raman spectrum of **1** by comparison with the Raman spectrum recorded at a nonresonant wavelength (i.e., 785 nm, Figure S1) and a clear excitation wavelength dependence on the relative intensities of individual bands (Figure S18).

At all wavelengths examined (which span both visible absorption bands), vibrational modes are observed at 1608, 1571, 1485, 1304, 1272, 1159, and 1029 cm^{-1}, which are assigned to pyridyl based vibrations by comparison with the Raman spectrum of $[Fe(bpy)_3]^{2+}$ (1608, 1565, 1492, 1322, 1278, 1175, 1026 cm^{-1}).[29] The modes at 1464, 1375, 1304, 1288, 1228, and 1076 cm^{-1} are assigned as C−H vibrational modes of the alkyl amine backbone on the basis of the isotope shifts observed in the spectra of d_5-**1** (Figure S19) in which the alkyl hydrogens are exchanged for deuterium. The 1608 cm^{-1} mode of **1** is more intense relative to the 1571 cm^{-1} mode at λ_{exc} 355 and 400.8 nm (i.e., absorption band II), however, at λ_{exc} 449 and 473 nm (i.e., absorption band I) the reverse is the case with the 1571 cm^{-1} mode more intense than the 1608 cm^{-1} mode. Overall, the spectra are typical for Fe^{II} and Ru^{II} polypyridyl complexes,[29−31] and the visible absorption bands of **1** are assigned as ^{1}MLCT with transfer of charge from Fe^{II} to the pyridyl rings; albeit with a substantial contribution from the ligand's alkyl amine backbone. The enhancement of alkyl amine modes is advantageous as it allows for changes in the first coordination sphere to be monitored in detail (*vide infra*). A similar excitation wavelength dependence of the resonance Raman spectrum of **2** was observed (Figure S20). The resonance Raman spectra of **1** and **2** in acetonitrile at λ_{exc} 473 nm are shown in Figure 8. The spectra are essentially identical in the regions between 1400 and 1700 cm^{-1} and 1000 and

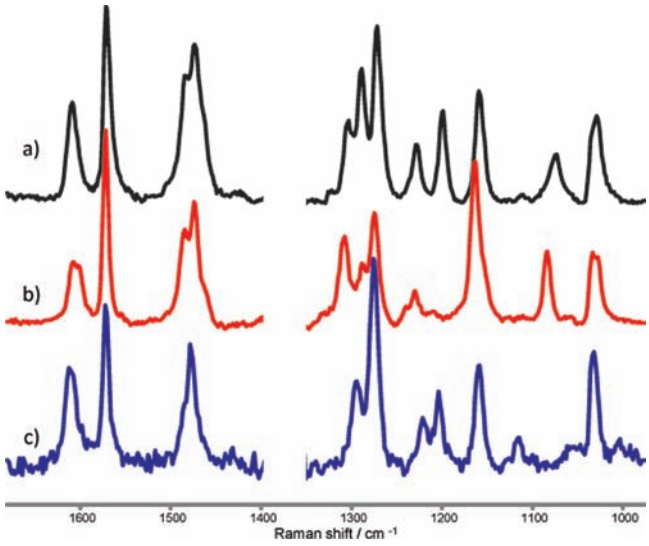

Figure 8. Resonance Raman spectra of (a) **1**, (b) **2** at λ_{exc} 473 nm, and (c) **3** at λ_{exc} 449 nm (0.1 mM) in acetonitrile. Spectra are solvent subtracted, residual solvent bands are masked.

1100 cm^{-1} with only minor shifts in the pyridyl based modes. As expected the modes due to the alkyl amine backbone of the ligand are distinctly different in the range 1200−1400 cm^{-1}.

For complex **3** vibrational modes are observed at 1610, 1572, 1477, 1327, 1275, 1159, and 1033 cm^{-1} (Figure 8), all of which are assigned to pyridyl based vibrations by comparison with the Raman spectrum of $[Fe(bpy)_3]^{2+}$ (1608, 1565, 1492, 1322, 1278, 1175, 1026 cm^{-1}).[29] The modes at 1296, 1223, and 1207 cm^{-1} are assigned to the alkyl amine backbone based on comparison with the resonance Raman spectra of **1**. The band at 1003 cm^{-1} is assigned to a phenyl ring vibrational mode.

Resonance Raman Spectroscopy in Water. The resonance Raman spectra of **1** in water (pH 7.6) and acetonitrile are shown in Figure 9 and Figure S21. The spectra are similar, however there are a number of differences in the position and the relative intensities of certain modes. The most notable changes in the spectrum are observed in the region 1200−1400 cm^{-1}. The bands that change

dx.doi.org/10.1021/ic201879b | *Inorg. Chem.* 2012, 51, 900−913

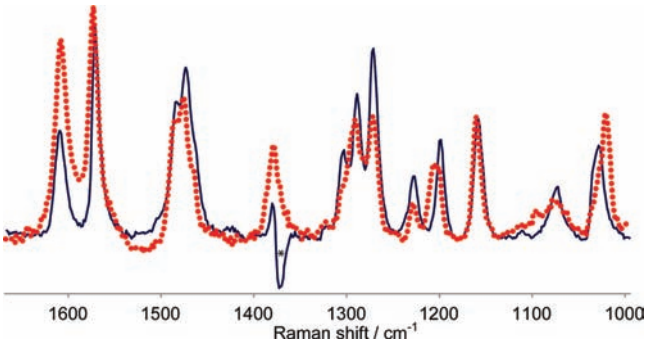

Figure 9. Resonance Raman spectra at λ_{exc} 473 nm of **1** in acetonitrile (solid line) and water (dotted) at pH 7.6. (*) Indicates distortion due to imperfect solvent subtraction. For additional spectra of **1** in water with added acetonitrile and with added NaCl see Figure S22.

are modes of the alkyl amine ligand backbone. The changes in these modes indicate that the coordination sphere of the complex, such as Fe−N bond lengths, is changed slightly, i.e., the conformation of the alkyl amine ligand backbone, as expected due to the replacement of a CH_3CN ligand for a hydroxido ligand.

pH Dependence of the Resonance Raman Spectroscopy of 1. The resonance Raman spectra of **1** in aqueous solution were obtained over the range pH 2.4 to 11.7 with SO_4^{2-} as internal reference (Figure 10). At pH 7.6, the bands are most

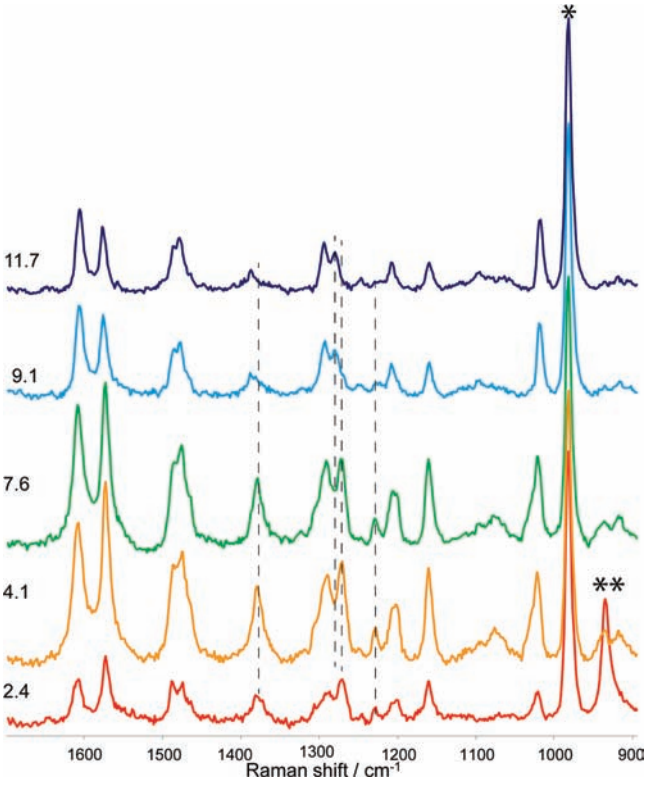

Figure 10. Resonance Raman spectra of **1** in water at various pH values at λ_{exc} 473 nm at 0.5 mM (spectra are normalized to the 981 cm^{-1} band of the 0.05 M SO_4^{2-} internal reference). For the corresponding UV/vis absorption spectra of the solutions used to obtain the Raman spectra see Figure 6a. (*) SO_4^{2-}, (**) ClO_4^-.

intense with respect to the spectra obtained at higher and lower pH. Between pH 2 and 4, the intensity of the vibrational modes of **1** decrease, and below pH 2 they become too weak to be detected. This is consistent with the decrease in the UV/vis absorption that is observed over this pH range and ^1H NMR spectra showing dissociation of the ligand at low pH (*vide supra*). Although the absolute intensity decreases as the pH is lowered, the spectrum itself is otherwise unchanged with the relative intensities of individual bands remaining constant. Above pH 8 a substantial change in the spectrum was observed. The modest decrease in intensity over this pH range is consistent with the decrease in absorbance at 473 nm. Furthermore, the change in the relative intensity of the 1605 cm^{-1} and 1571 cm^{-1} band is most probably due to the bathochromic shifting of band I. Importantly, there is a clear change in the spectrum in the region 1100−1300 cm^{-1} which cannot be ascribed to changes in the UV/vis absorption spectrum, specifically the modes at 1375, 1304, and 1228 cm^{-1} either are lower in relative intensity or are absent at high pH (>8). The differences between the spectra recorded at low and high pH can be assigned, therefore, to significant changes in the coordination of the ligand.[25] The resonance Raman spectrum of **3** in acetonitrile and in water at pH 6.5 are more similar to the spectrum of **1** in water at pH 9.1 than the spectrum of **1** in water at pH 7.6 (Figure S23). This indicates that on going from low to high pH the N4Py ligand of complex **1** switches from penta- vs tetra-dentate, i.e. at high pH one of the pyridine rings dissociates from the Fe^{II} center with coordination of an additional hydroxido ligand.

The resonance Raman spectra of **2** in aqueous solution were obtained also between pH 2.1 and 11.4 with SO_4^{2-} as internal reference (Figures S24 and S25). Confirmation that the CH_3CN ligand of **2** is fully dissociated in water is obtained from the correspondence of the spectrum of **2** in water with that of the in situ prepared complex (from $FeSO_4$ and MeN4Py ligand, Figures S26 and S27). In addition, as for the UV/vis absorption spectrum of **2** in aqueous solution, addition of 1 vol% of acetonitrile leads to a change to a resonance Raman spectrum identical to that observed for **2** in acetonitrile (Figure S28).

At pH 7.5, 4.5, and 2.1 the bands of **2** are most intense with respect to the spectra obtained at higher pH (Figure S24 and S25). This is consistent with the UV/vis absorption spectrum, which is essentially unchanged over this pH range (Figure 7a). Above pH 8 the intensity of the bands decreases, consistent with the decrease in absorbance over this pH range and as observed for **1**, substantial changes in both relative intensity and band position were observed. In particular the bands associated with the alkyl amine ligand backbone are most affected, indicating that a change in the ligand conformation and also coordination mode occurs between pH 7 and 9. At pH 11 the overall intensity is decreased consistent with ligand dissociation at this pH.

Electrochemistry. Cyclic voltammetry of **1** shows a reversible oxidation at 1.1 V in acetonitrile and at ca. 0.4 V in water (pH 6.5), respectively (Figure 11). Addition of water (1 vol%) to an acetonitrile solution of complex **1** renders the otherwise reversible oxidation irreversible with a new reduction wave observed at 0.6 V on the return cycle (Figure 11a). The correspondence of the potential of the new reduction wave with that of the oxidation potential of **1** in water (under acidic conditions) indicates that although the coordination of CH_3CN is favored in the Fe^{II} oxidation state, when oxidized to Fe^{III} the CH_3CN ligand is displaced readily by H_2O.[32] This is reversed upon reduction of Fe^{III} back to the Fe^{II} oxidation state as expected based on the preference of nitrogen donor ligands for low-spin Fe^{II} due to back bonding stabilization.[33]

dx.doi.org/10.1021/ic201879b | *Inorg. Chem.* 2012, 51, 900−913

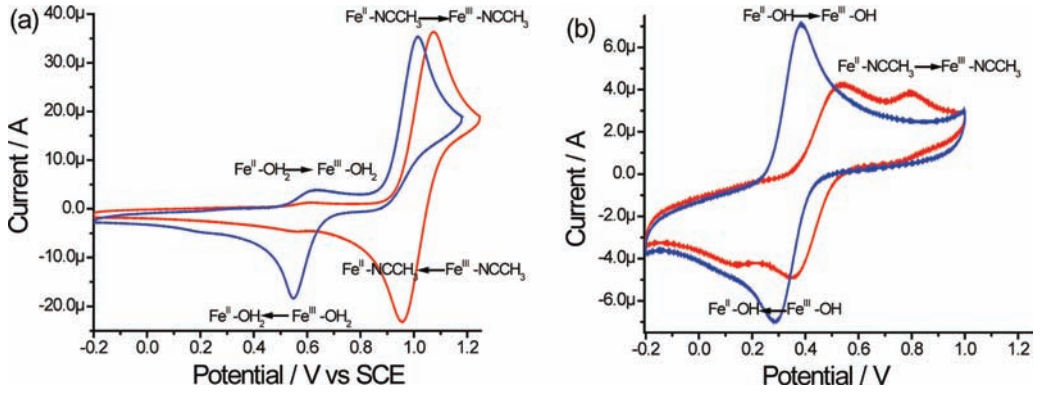

Figure 11. Cyclic voltammograms of **1** (0.5 mM) (a) in acetonitrile (0.1 M $TBAPF_6$) (red line) and after addition of 1 vol% water (blue line); (b) in water (0.01 M KNO_3) (blue line) and after addition of 1 vol% acetonitrile (red line). Scan rate 0.1 V s^{-1}.

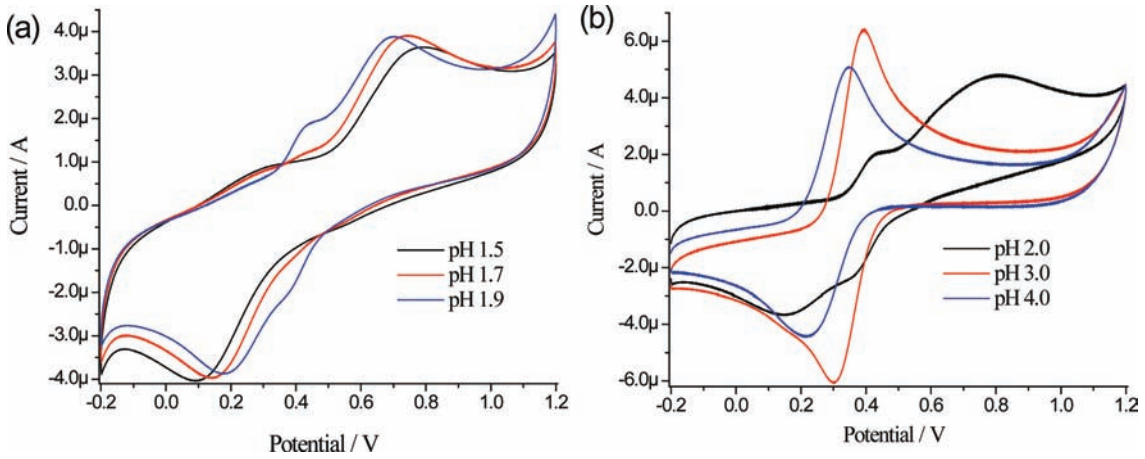

Figure 12. Cyclic voltammograms of **1** (0.5 mM) in water (10 mM KNO_3) at pH (a) 1.5, 1.7, and 1.9, (b) 2.0, 3.0, and 4.0. Scan rate: 0.1 V s^{-1}.

Although from UV/vis absorption spectroscopy it is apparent that addition of acetonitrile to an aqueous solution of **1** results in immediate reversion to a CH_3CN bound complex (Figure 5a), the effect on the cyclic voltammetry is not so clear (Figure 11b). Addition of 1 vol% of acetonitrile to an aqueous solution of **1** would result in a shift of the oxidation wave to ca. 1 V. Instead, only a modest shift of 100 mV of the oxidation wave to more positive potentials and the appearance of a new irreversible oxidation wave at ca. 0.8 V are observed. These observations can be rationalized by considering that the CH_3CN and aqua ligands exchange rapidly in aqueous solution and although the equilibrium lies in favor of the CH_3CN coordination, the rates of the forward and reverse reactions are sufficiently high with respect to scan rate to result in a less positive oxidation wave. Similar behavior is observed for **2** also (Figures S31).

The cyclic voltammetry of **3** in acetonitrile shows a single quasi-reversible redox wave for the Fe^{III}/Fe^{II} couple at 1.15 V (Figure S32). Addition of water (<1 vol%) to an acetonitrile solution results in the oxidation wave at 1.15 V becoming irreversible and an increase in the intensity of the subsequent reduction wave at 0.63 V and a smaller reduction wave at 0.30 V. In water (pH 6.5) the oxidation potential of **3** is 0.44 V (Figure S32).

pH Dependence of the Redox Chemistry of 1, 2, and 3. As for the ^1H NMR, UV/vis absorption, and resonance Raman spectroscopy, the redox chemistry of **1** and **2** in water is pH dependent.

pH Dependence of the Cyclic Voltammetry of 1. Between pH 2.5 and 5 only one redox wave (species **A** in Figure 14) is observed within the accessible potential window (Figure 12). The $E_{1/2}$ increases linearly below pH 4 (see Pourbaix plot, Figure 14). Below pH 2.5 an additional electrochemically irreversible redox wave is observed assigned to ligand dissociated iron(II) species (e.g., $Fe(H_2O)_6^{2+}$, by comparison with the $FeSO_4$ under the same conditions, Figure S35).

Above pH 5, a second reversible redox wave (species **B**, Figure 14) at lower potential (~100 mV) is observed (Figure 13a). At pH 8 only the redox wave at ca. 50 mV is observed. Notably the stability of species **A** in the Fe(III) state is considerably less than that of species **B** (i.e., the redox wave at 300 mV becomes increasingly irreversible as the pH is raised).

Above pH 9, the $E_{1/2}$ decreases with a pH dependence consistent with a $1e^-/1H^+$ coupled process. At pH > 11 the complex is unstable manifested in a decrease in the current density of the redox wave, and at pH > 13, decomplexation is complete (Figure 13b). The decomplexation is in agreement with the observation of noncoordinated ligand by ^1H NMR spectroscopy (*vide supra*).

The Pourbaix plot for **1** in aqueous solution (Figure 14) indicates that two distinct species are present in solution between pH 5 and 8. Furthermore between pH 1.8 and 4.6 and above pH 9, the reduction potential is pH dependent in a manner consistent with a $1e^-/1H^+$ coupled redox process (slope is ~ −59 mV/pH). For the species present at low pH (species **A**), the reduced form (i.e., the Fe^{II} complex) has a pK_a of 4.5, while for the oxidized form (i.e., the Fe^{III} complex) the pK_a is 1.9. For the species present at higher pH values (species **B**),

dx.doi.org/10.1021/ic201879b | *Inorg. Chem.* 2012, 51, 900−913

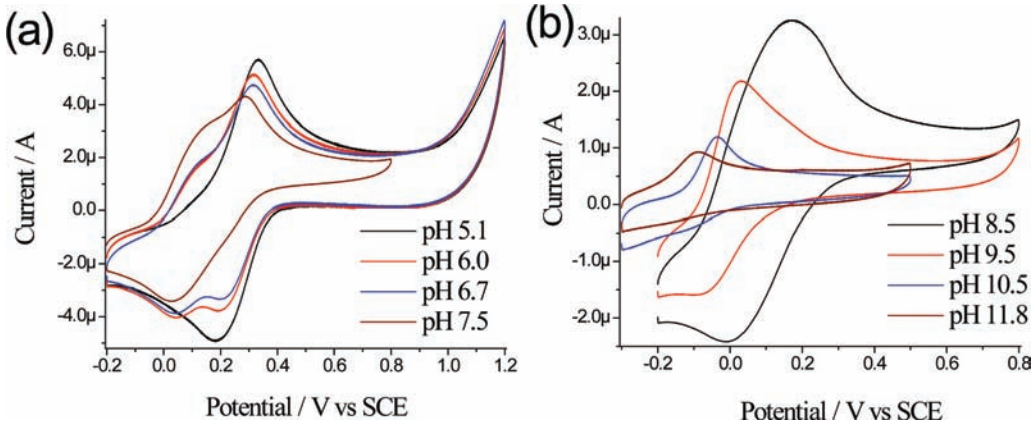

Figure 13. Cyclic voltammograms **1** (0.5 mM) in water (10 mM KNO_3) at pH (a) 5.1, 6.0, 6.7, and 7.5 and (b) 8.5, 9.5, 10.5, and 11.8. Scan rate: 0.1 V s^{-1}.

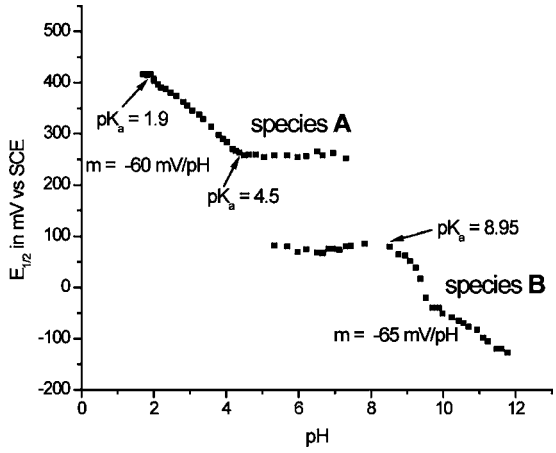

Figure 14. Pourbaix plot for **1** in water (10 mM KNO_3).

the pK_a of the Fe^{II} state is >12 while for the Fe^{III} state the pK_a is 8.95.

At pH values less than pH 3 and greater than pH 10, an additional factor is ligand dissociation (as confirmed by ^1H NMR spectroscopy, *vide supra*). For clarity the redox chemistry of the dissociated iron is not described in the Pourbaix plot (Figure 14). Importantly, pH jumping experiments show that over short periods the ligand dissociation observed at low and high pH is fully reversible (Figures S36 and S37). Indeed the initial pH and direction of pH change was found to have no influence on the pH dependence observed. Furthermore, the cyclic voltammetries of **1** and complex **4** (which has a chlorido ligand in place of the CH_3CN ligand) are identical at all pH values confirming that the complexes are fully solvated (Figure S29).

pH Dependence of the Cyclic Voltammetry of 2 and 3. Complex **2** shows electrochemical behavior similar to **1**. Overall the stability of **2** with respect to full ligand dissociation is greater at low and high pH than observed for **1** (Figure S33a). By contrast, the oxidation potential of **3** is only moderately pH dependent with an increase in $E_{1/2}$ below pH 4.5 which may indicate that the pK_a of **3** is at ca. 4.5 (Figure S33b). Below pH 3 and above 8.5 the complex was found to be highly unstable with respect to ligand dissociation, in agreement with the ^1H NMR spectra of **3** in D_2O (Figure S13, *vide supra*).

Electrospray Ionization Mass Spectrometry (ESI-MS). ESI-MS is a widely applied technique in the characterization of first row transition metal complexes allowing for study under a wide range of solvent conditions.[34] In the present study, however, obtaining signals in pure or buffered aqueous solutions was found to be impractical due to poor spray formation. Therefore, ^{t}BuOH/H_2O mixtures were employed to allow for a stable electrospray. Because of the solvent dependence observed for the Fe^{II}(N4Py) complexes (UV/vis absorption spectroscopy, *vide supra*), control experiments were performed to confirm that the species present in ^{t}BuOH/H_2O were the same as those present in water. From the UV/vis absorption spectra and cyclic voltammetry (Figure S38) it is apparent that at the 25 vol% of ^{t}BuOH there is a minor change observed compared to in water alone, which is possibly due to oxidation to the Fe^{III} state. A further consideration in performing and interpreting the ESI-MS data obtained is the limited control over pH achievable in the spray due to the nature of the ESI technique itself and the potential for in situ redox reactions and oxidation by oxygen.[17] Notwithstanding these considerations,[35] ESI-MS indicated the presence of several structures in solution that are consistent with other spectroscopic and electrochemical data.

The ESI-MS spectrum of **1** in ^{t}BuOH/H_2O (1:4 v/v) at pH 2, 6, and 11 (Figures S39, S40 and S41, respectively) shows that, at pH 2 and 6, the CH_3CN ligand is dissociated with several major ions observed including $[Fe^{II}N4Py(OH_2)]^{2+}$/$[Fe^{III}N4Py(OH)]^{2+}$ (m/z 220.2),[36] $[Fe^{III}N4Py(^tBuO)]^{2+}$ (m/z 248.3), $[Fe^{II}N4Py](ClO_4)^+$ (m/z 522.3), $[Fe^{III}N4Py(OH)](ClO_4)^+$ (m/z 539.3), and $[Fe^{III}N4Py(^tBuO)](ClO_4)^+$ (m/z 595.3). At pH 11, signals assigned to $[Fe^{II}N4Py(OH)]^+$ (m/z 440) and $[Fe^{III}N4Py(OH)_2]^+$ (m/z 457) are observed primarily. The observation of species in the Fe^{III} oxidation state is not unexpected given the relatively low redox potential in water (*vide supra*) and the propensity for the complexes to be oxidized by O_2. It should be noted that the corresponding Fe^{II} complex of $[Fe^{III}N4Py(OH)_2]^+$ is neutral and hence its presence in solution is not observable by mass spectrometry.

DISCUSSION

In the present study the pH dependence of the electrochemical and spectroscopic properties of **1** are compared and contrasted with those of the related complexes **2** and **3** (Figure 1). The complexes were characterized by single crystal X-ray analysis, ^1H NMR, and Raman spectroscopy. The structures of complexes **1**−**3** observed in the solid state (see X-ray Crystallography section) are retained in acetonitrile solution as confirmed by the correspondence between solution and solid state (nonresonant) Raman spectroscopy. As expected for

dx.doi.org/10.1021/ic201879b | *Inorg. Chem.* 2012, 51, 900−913

low-spin Fe^{II} complexes, in acetonitrile-d_3 **1**, **2**, and **3** are EPR silent and exhibit a diamagnetic ^1H NMR spectrum between 0 and 10 ppm. The solution properties of these complexes were studied by ^1H NMR, UV/vis absorption, Raman and resonance Raman spectroscopy, electrochemistry, and ESI-MS in both aprotic (acetonitrile) and protic (water) solvents. The multitechnique approach taken allows for a deeper understanding to emerge of both the coordination chemistry and electronic structure of the complexes in aqueous and nonaqueous media and importantly the pH dependence of the equilibria between the various species present in solution, as summarized in Schemes 1 and 2 below.

In aqueous/acetonitrile solutions of **1** and **2**, an equilibrium between the CH_3CN and H_2O bound complexes is such that in the Fe^{II} oxidation state coordination of CH_3CN is favored,

Scheme 1. Species and Equilibria Occurring in Aqueous/Acetonitrile Mixtures for 1 and 2

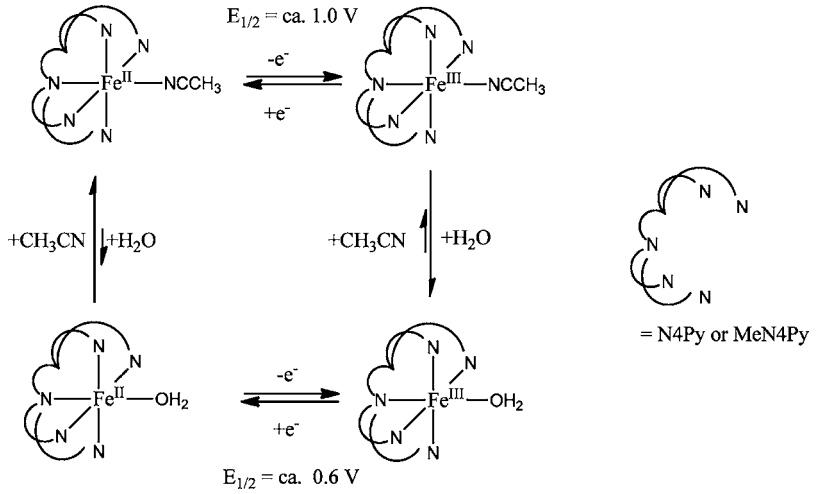

Scheme 2. Species and Equilibria Occurring in Aqueous Solution for 1 and 2 (Potentials and pKa Values Are Approximate; See Text for Details)

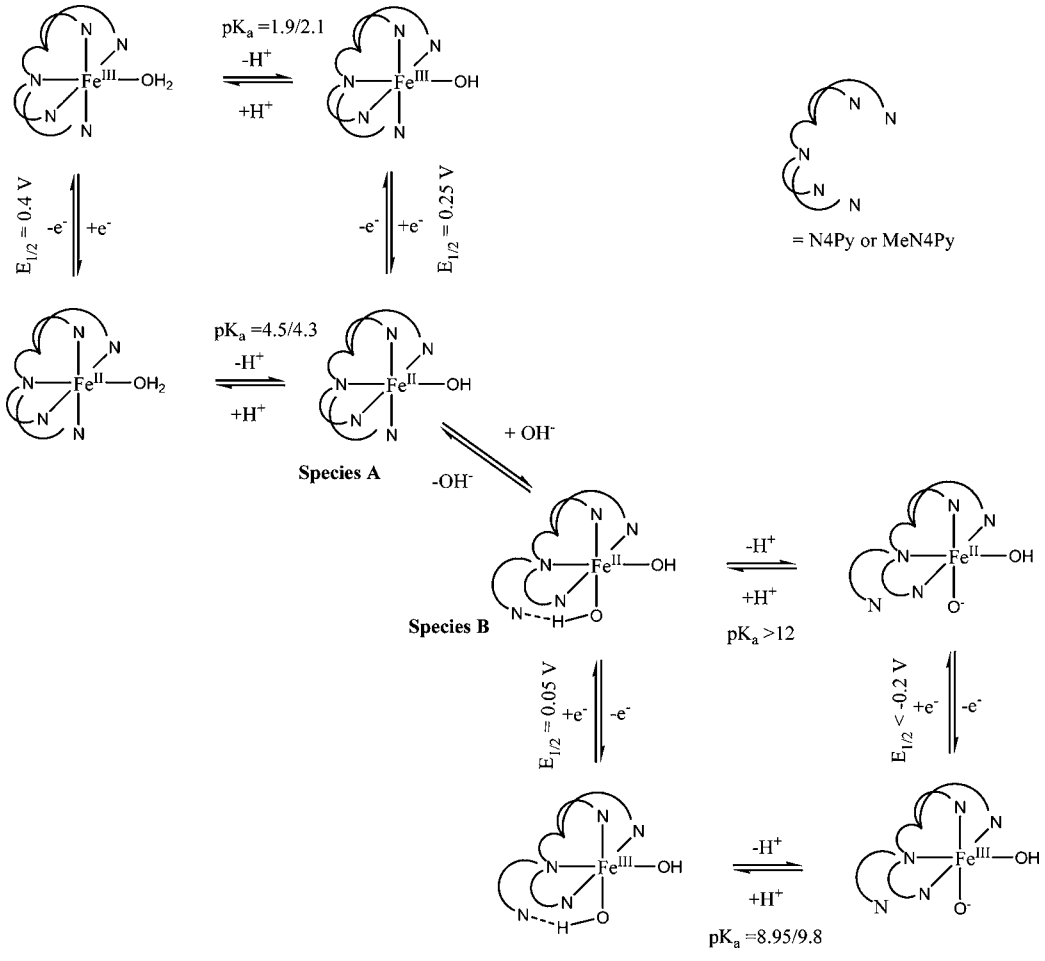

dx.doi.org/10.1021/ic201879b | Inorg. Chem. 2012, 51, 900–913

whereas in the Fe^{III} state coordination of water dominates the equilibrium. Indeed, even millimolar amounts of water are sufficient to displace the CH_3CN ligand in the Fe^{III} state. The effect of addition of acetonitrile to aqueous solutions of the complexes on their UV/vis absorption spectrum shows that the equilibrium favors CH_3CN with respect to H_2O coordination in the Fe^{II} state. However, from cyclic voltammetry it is apparent that the equilibrium between the two states is reasonably fast on the electrochemical time scale (tens of milliseconds). For **3** an opposite behavior is observed with facile displacement of at least one of the CH_3CN ligands by an hydroxido or aquo ligand.

For all three complexes, ligand dissociation is a key feature of their aqueous chemistry at low (<pH 3) and high (>pH 9) pH and is readily observed by ^{1}H NMR spectroscopy and electrochemistry. The stability of the complex with regard to ligand dissociation is in the order **3** < **1** < **2**, with **2** forming the most stable complexes. The discussion below will, however, consider pH ranges in which the ligands are coordinated to the Fe^{II}.

Complex 1 in Aqueous Solutions. The species present in aqueous solutions of **1** are highly pH dependent. It is certain that, upon dissolution in water, the CH_3CN or chlorido ligands (in the case of **4**) dissociate fully and the complex is solvated as confirmed by comparison with in situ formation of the complex by mixing free ligand with $FeSO_4$. An equilibrium is established between two distinct species in solution (species **A** and **B**, Scheme 2) in addition to acid/base chemistry at low (ca. pH 2−4) and high (ca. pH 9) pH and ultimately ligand dissociation at below pH 2.5 and above pH 9. This is most clearly seen in the Pourbaix plots (Figure 14 and S33) and the pH dependence of the UV/vis absorption spectrum (Figure 6).

The pH dependence of the resonance Raman spectrum (Figure 10) tracks, in terms of overall intensity, the changes observed in the absorption spectrum, i.e., the lower the absorbance the weaker the spectrum and vice versa, and the relative intensity of the Raman scattering from each of the vibrational modes varies in accordance with blue/red shifts in the main absorption bands. Furthermore the pyridyl modes, in particular the band at 1605 cm^{-1}, are typical of resonance enhancement by excitation into a ^{1}MLCT band for a low-spin Fe^{II} complex.[30] A more subtle change is observed also in the vibrational structure associated with the alkyl amine ligand backbone. The concomitant disappearance and appearance of modes is indicative of two distinct species (labeled **A** and **B**, Scheme 2) present in a pH-dependent equilibrium. The range over which the change in the relative contribution of each species to the total signal in the Raman spectrum is coincident with the changes observed in the UV/vis absorption spectra between pH 7 and 9 (Figure 6) and the appearance of two distinct redox waves in the cyclic voltammetry. The differences in the Raman spectra of the two species together with the pK_a's of the two species lying outside of the pH 7−9 region indicates that the changes observed in this pH range by ^{1}H NMR, UV/vis absorption and Raman spectroscopy, and by cyclic voltammetry are due to a structural change in the complex; specifically the detachment of one of the pyridyl rings from the Fe^{II} at high pH (>ca. 8) (Scheme 2).[37]

Assignment of the Molecular Structure of the Species Present at Low and High pH. The close correspondence of the resonance Raman spectrum of **1** in water at pH 6−7 and in acetonitrile together with confirmation that the CH_3CN ligand of **1** dissociates fully in water support the assignment of species **A** (Scheme 2) as $[Fe^{II}(N4Py)(OH)]^+$. The observation of a m/z signal at 220 is consistent with this assignment. The changes observed in the ligand alkyl amine modes compared with species **A** and with **1** in acetonitrile solution and the decrease in redox potential are consistent with the assignment of the structure $[Fe^{II}(N4Py)(OH)_2]$ to species **B**. This assignment is supported further by the correspondence of the Raman spectra of **3** with species **B**. Mass spectrometry, despite the caveats mentioned in the Results section, supports, albeit tentatively, the assignment of the species made in Scheme 2, although the major signals observed are the Fe^{III} forms of species **A** and **B**.

Spin State of Aqueous Species A and B. Although a priori one would expect that the Fe^{II} complex present in aqueous solution would be in a high-spin state (typically the quintet state), ^{1}H NMR, UV/vis absorption, and resonance Raman spectroscopy suggest that for **1** there is a substantial (ca. 50%) proportion of the complex in a low-spin (singlet) state.

For **1**, the ^{1}H NMR spectrum shows a strong paramagnetic downfield shift consistent with the complex in a nonsinglet ground state (Figure 3). However at pH < 8 the resonances are broadened and it is clear that of the two species (**A** and **B**) present in a pH-dependent equilibrium, species **B** (high pH) shows much sharper resonances than species **A**. The time scale of ^{1}H NMR spectroscopy (ms) results in a spectrum that is the weighted average of the species present in solution. Hence, the spectral broadening indicates that species **A** and **B** show spin equilibrium with relatively equal amounts (based on molar absorptivities) of singlet spin and, presumably, quintet species.

UV/vis absorption and Raman spectroscopy represent shorter experimental time scales (fs) and hence each species contributes to the spectrum in an additive manner, i.e., the spectra are a sum of the individual contributions. The UV/vis absorption spectra of **1** in aqueous solution (Figure 6) is consistent with the conclusions drawn from the ^{1}H NMR spectral data (Figure 3). A red shift in the visible bands is observed and a decrease in absorptivity compared with the spectrum in acetonitrile is observed, however the resonance Raman spectrum shows that, certainly in the case of species **A** (above pH 4) and species **B**, at least 50% is in a low-spin state. Below pH 4 species **A** is protonated and the decrease in the visible absorption indicates that the high-spin state is dominant for the protonated complex (Scheme 3).

Comparison of 1 with 2. In complex **2**, the N4Py ligand is modified with a methyl group at the tertiary alkyl carbon of the ligand (MeN4Py). This change to the N4Py ligand was not expected to show a substantial effect on the electronic properties compared to N4Py, but to introduce greater rigidity (through steric hindrance) to the ligand when complexed to Fe^{II}. Surprisingly this modification was found to have a clear effect on the complex's electronic properties and improved the stability of **2** with respect to ligand dissociation in aqueous solutions below pH 2 and above pH 9 compared with **1**. The difference in stability between **1** and **2** is not due to the replacement of the sensitive tertiary proton in the alkyl amine backbone of **1**, but more likely due to steric effects of the methyl group, which stabilizes the complex by pushing the two adjacent pyridyl rings toward each other and the Fe^{II} center. For **2** the introduction of the methyl group in the ligand alkyl amine backbone decreases the Fe−N ligand bond lengths and increases the stability further especially at low pH. The stability of the ligand and reversibility of the ligand dissociation is confirmed by the full reversibility observed in pH jumping experiments (Figures S36 and S37).

Spin State of Aqueous Species (2)A and (2)B. Overall the aqueous chemistry of **2** mirrors that of **1**, however there are several important differences. In contrast to **1** the ^{1}H NMR spectrum of **2** at pH < 8 is an essentially diamagnetic ^{1}H NMR

dx.doi.org/10.1021/ic201879b | Inorg. Chem. 2012, 51, 900−913

Scheme 3. Relative Ratios of Singlet and High-Spin State Species for Each Species for 1 and 2

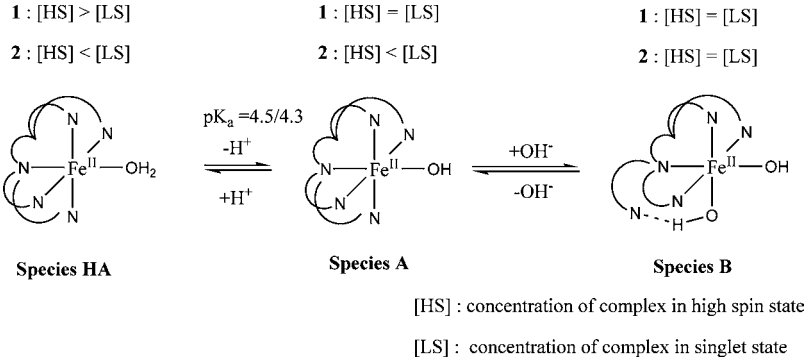

spectrum with only minor line broadening. At higher pH values (pH > 8) resonances shifted to the same extent as for **1** are observed. For **1** the decrease in absorptivity in water compared with acetonitrile is ca. 50%. For **2** the difference in absorptivity between water and acetonitrile is ca. 20% only. Taken together these data indicate that for species (**2**)**A** the singlet state is favored over a high-spin species at pH < 8. At higher pH the UV/vis absorption decreases, consistent with a shift toward a high-spin species (**2**)**B**. By comparison with the absorptivity of **1** at high pH, it appears that species **B** and species **2**(**B**) show similar equilibria between low- and high-spin states.

Comparison of 1 and 2 with 3. In the case of **3**, one of the pyridine rings of the ligand is replaced by a phenyl group (Bn-N3Py) to increase the number of coordination sites on the complex available to solvent and to estimate the effect of partial ligand dissociation on the spectroscopic and electrochemical properties of **1**. In acetonitrile solution both of the free coordination sites are occupied by CH_3CN ligands. The resonance Raman spectrum of **3** in acetonitrile (Figure 8) is consistent with a low-spin Fe^{II} polypyridyl complex in particular with regard to the relative intensity of the 1610 cm^{-1} mode.[30] In aqueous acetonitrile solutions, **3** exhibits behavior similar to that as observed for **1** and **2** except that in this case two solvent molecules are exchanged upon change of oxidation state. In aqueous media the CH_3CN ligands are displaced by either aquo and/or hydroxido ligands. The tetradentate ligand is relatively ineffective in forming a stable complex except at intermediate pH values (pH 4−8) with ligand dissociation apparent both in the ^1H NMR spectra and in the cyclic voltammetry at pH < 4 and pH > 8.

It is apparent from the pH dependence of the electrochemistry, ^1H NMR spectroscopy (in which only a single paramagnetic species with reasonably sharp resonances is observed in D_2O) and UV/vis absorption spectroscopy that in aqueous solution complex **3** solvates to form a high-spin Fe^{II} complex. For **3**, the blue shift and large decrease in absorption compared with that in acetonitrile solution is consistent with a high-spin Fe^{II} species. Comparison of the Pourbaix plots (Figure 14) for **1** (and **2**, Figure S33a) with that of **3** (Figure S33b) would indicate that the species present at low pH (i.e., species **A**) would resemble **3** most. However, the possibility of hydrogen bonding interaction between the free pyridyl ring and the coordinated hydroxide could account for the difference in redox potential of **3** and species formed by **1** and **2** at high pH.

CONCLUDING REMARKS

In this contribution we have undertaken a combined spectroscopic and electrochemical study of the oxidation catalyst **1** in acetonitrile and aqueous solutions. The results were compared and contrasted with the analogous complexes **2** and **3**. Overall the pH dependence of **1** (and **2**) shows that in addition to the expected acid/base chemistry, two species (**A** and **B**) are present in pH-dependent equilibrium. Importantly there are additional equilibria for species **A** (and **B**) between the low- (singlet) and high-spin (e.g., quintet) states. The extents of the equilibria are dependent on pH and on molecular structure with **2** showing increased stabilization of the singlet state especially for species (**2**)**A** compared with species **A** (formed from **1**). This is especially the case at low pH (< 4). For **3** only a single high-spin species is present in water.

For **1** in aqueous solution the interconversion between the singlet and, presumably, quintet states may be key to understanding the ability of **1** to engage in oxidative DNA cleavage with $^3O_2$. The interconversion between the singlet and higher spin states would be expected to involve an intermediate triplet state, the transient formation of which would facilitate electron transfer to $^3O_2$, the first step in the cleavage of DNA by **1** with $^3O_2$. This conclusion is consistent with our recent observation[13] that visible and near-UV light can enhance the activity of **1** in cleaving DNA in which the transient population of the triplet state of **1** ($[N4PyFe^{II}(OH)]^+$) following photoexcitation in the ^{1}MLCT states would be expected.

In conclusion, the combined electrochemical and spectroscopic study of the pH dependence of **1**−**3** demonstrates the remarkably complex coordination chemistry that these species exhibit in aqueous solution. The results reported form a solid foundation on which a mechanistic understanding can be built of the activity of complexes such as **1** in oxidation catalysis with molecular oxygen and the complexes formed after reaction of high valent (Fe^{IV}) oxo complexes with organic substrates.

ASSOCIATED CONTENT

Supporting Information

Details of synthesis and characterization of ligands and complexes, X-ray structural analysis, additional FTIR, Raman, ^1H NMR, and UV/vis absorption spectral, electrochemical, and ESI-MS data. This material is available free of charge via the Internet at http://pubs.acs.org.

AUTHOR INFORMATION

Corresponding Author

*E-mail: w.r.browne@rug.nl.

■ ACKNOWLEDGMENTS

We thank the University of Groningen for a Ubbo Emmius Scholarship (A.D., Q.L.), The Netherlands Organization for Scientific Research (*NWO*) for a VIDI grant (700.57.428, H.L., W.R.B.) and The Netherlands Fund for Technology and Science *STW* (11059, W.R.B.). Dr M. Lutz and Prof A. L. Spek are kindly acknowledged for obtaining the X-ray structure of complex **2**.

■ REFERENCES

(1) (a) Umezawa, H.; Maeda, K.; Takeuchi, T.; Okami, Y. *J. Antibiot.* **1966**, *19*, 200−209. (b) Hecht, S. M. *Bleomycin: Chemical, Biochemical and Biological Aspects*; Springer: New York, 1979. (c) Pogozelski, W. K.; Tullius, T. D. *Chem. Rev.* **1998**, *98*, 1089−1108. (d) Burger, R. M. *Chem. Rev.* **1998**, *98*, 1153−1170. (d) Claussen, C. A.; Long, E. C. *Chem. Rev.* **1999**, *99*, 2797−2816. (f) Hecht, S. M. *J. Nat. Prod.* **2000**, *63*, 158−168.

(2) (a) Stubbe, J.; Kozarich, J. W.; Wu, W.; Vanderwall, D. E. *Acc. Chem. Res.* **1996**, *29*, 322−330. (b) Chen, J. Y.; Stubbe, J. *Nat. Rev. Cancer* **2005**, *5*, 102−112.

(3) (a) Murugesan, N.; Hecht, S. M. *J. Am. Chem. Soc.* **1985**, *107*, 493−500. (b) Padbury, G.; Sligar, S. S. *J. Biol. Chem.* **1985**, *260*, 7820−7823. (c) Heimbrook, D, C.; Carr, S. A.; Mentzer, M, A.; Long, E, C.; Hecht, S, M. *Inorg. Chem.* **1987**, *26*, 3835−3836.

(4) (a) Petering, D. H.; Byrnes, R. W.; Antholine, W. E. *Chem. Biol. Interact.* **1990**, *73*, 133−182. (b) Feig, A. L.; Lippard, S. J. *Chem. Rev.* **1994**, *94*, 759−805. (c) Loeb, K. E.; Zaleski, J. M.; Westre, T. E.; Guajardo, R. J.; Mascharak, P. K.; Hedman, B.; Hodgson, K. O.; Solomon, E. I. *J. Am. Chem. Soc.* **1995**, *117*, 4545−4561. (d) Que, L. Jr. *J. Biol. Inorg. Chem.* **2004**, *9*, 684−690. (e) Kryatov, S. V.; Rybak-Akimova, E. V.; Schindler, S. *Chem. Rev.* **2005**, *105*, 2175−2226. (f) Decker, A.; Rohde, J. U.; Klinker, E. J.; Wong, S. D.; Que, L. Jr.; Solomon, E. I. *J. Am. Chem. Soc.* **2007**, *129*, 15983−15996. (g) Chow, M. S.; Liu, L. V.; Solomon, E. I. *Proc. Natl. Acad. Sci. U.S.A.* **2008**, *105*, 13241−13245.

(5) For examples, see: (a) Hertzberg, R. P.; Dervan, P. B. *J. Am. Chem. Soc.* **1982**, *104*, 313−315. (b) Hertzberg, R. P.; Dervan, P. B. *Biochemistry* **1984**, *23*, 3934−3945. (c) Guajardo, R. J.; Hudson, S. E.; Brown, S. J.; Mascharak, P. K. *J. Am. Chem. Soc.* **1993**, *115*, 7971−7977. (d) Silver, G. C.; Trogler, W. C. *J. Am. Chem. Soc.* **1995**, *117*, 3983−3993. (e) Pratviel, G; Bernadou, J.; Meunier, B. *Angew. Chem., Int. Ed.* **1995**, *34*, 746−769. (f) Mialane, P.; Nivorojkine, A.; Pratviel, G.; Azéma, L.; Slany, M.; Godde, F.; Simaan, A.; Banse, F.; Kargar-Grisel, T.; Bouchoux, G.; Sainton, J.; Horner, O.; Guilhem, J.; Tchertanova, L.; Meunier, B.; Girerd, J. J. *Inorg. Chem.* **1999**, *38*, 1085−1092. (g) Marchand, C.; Nguyen, C. H.; Ward, B.; Sun, J. S.; Bisagni, E.; Garestier, T.; Hélène, C. *Chem.—Eur. J.* **2000**, *6*, 1559−1563. (h) Kurosaki, H.; Maruyama, A.; Koike, H.; Kuroda, N.; Ishikawa, Y.; Goto, M. *Bioorg. Med. Chem. Lett.* **2002**, *12*, 201−203. (i) Mukherjee, A.; Dhar, S.; Nethaji, M.; Chakravarty, A. R. *Dalton Trans.* **2005**, 349−353.

(6) (a) Pitié, M.; Pratviel, G. *Chem. Rev.* **2010**, *110*, 1018−1059. (b) Sigman, D. S.; Mazumder, A.; Perrin, D. M. *Chem. Rev.* **1993**, *93*, 2295−2316.

(7) (a) Lubben, M.; Meetsma, A.; Wilkinson, E. C.; Feringa, B. L.; Que, L. Jr. *Angew. Chem., Int. Ed. Engl.* **1995**, *34*, 1512−1514. (b) Roelfes, G.; Branum, M. E.; Wang, L.; Que, L. Jr.; Feringa, B. L. *J. Am. Chem. Soc.* **2000**, *122*, 11517−11518. (c) Roelfes, G.; Vrajmasu, V.; Chen, K.; Ho, R. Y. N.; Rohde, J.; Zondervan, C.; la Crois, R. M.; Schudde, E. P.; Lutz, M.; Spek, A. L.; Hage, R.; Feringa, B. L.; Münck, E.; Que, L. Jr. *Inorg. Chem.* **2003**, *42*, 2639−2653.

(8) Gerard Roelfes, G.; Lubben, M.; Chen, K.; Ho, R Y. N.; Meetsma, A.; Genseberger, S.; Hermant, R. M.; Hage, R.; Mandal, S. K.; Young, V. G. Jr.; Zang, Y.; Kooijman, H.; Spek, A. L.; Que, L. Jr.; Feringa, B. L. *Inorg. Chem.* **1999**, *38*, 1929−1936.

(9) (a) Roelfes, G.; Lubben, M.; Hage, R.; Que, L. Jr.; Feringa, B. L. *Chem.—Eur. J.* **2000**, *6*, 2152−2159. (b) van den Berg, T. A.; de Boer, J. W.; Browne, W. R.; Roelfes, G.; Feringa, B. L. *Chem. Commun.* **2004**, 2550−2551.

(10) (a) van den Berg, T. A.; Feringa, B. L.; Roelfes, G. *Chem. Commun.* **2007**, 180−182. (b) Megens, R. P.; van den Berg, T. A.; de Bruijn, A. D.; Feringa, B. L.; Roelfes, G. *Chem.—Eur. J.* **2009**, *15*, 1723−1733. (c) Li, Q.; van den Berg, T. A.; Feringa, B. L.; Roelfes, G. *Dalton Trans.* **2010**, *39*, 8012−8021.

(11) (a) van den Berg, T. A.; de Boer, J. W.; Browne, W. R.; Roelfes, G.; Feringa, B. L. *Chem. Commun.* **2004**, 2550−2551. (b) Ray, K.; Lee, S. M.; Que, L. Jr. *Inorg. Chim. Acta* **2008**, *361*, 1066−1069.

(12) (a) Kaizer, J.; Klinker, E. J.; Oh, N. Y.; Rohde, J.-U.; Song, W. J.; Stubna, A.; Kim, J.; Munck, E.; Nam, W.; Que, L. Jr. *J. Am. Chem. Soc.* **2004**, *126*, 472−473. (b) de Visser, S. P.; Oh, K.; Han, A.-R.; Nam, W. *Inorg. Chem.* **2007**, *46*, 4632−4641. (c) Fukuzumi, S.; Kotani, H.; Lee, Y.-M.; Nam, W. *J. Am. Chem. Soc.* **2008**, *130*, 15134−15142.

(13) (a) Li, Q.; Browne, W. R.; Roelfes, G. *Inorg. Chem.* **2010**, *49*, 11009−11017. (b) Li, Q.; Browne, W. R.; Roelfes, G. *Inorg. Chem.* **2010**, *50*, 8318−8325.

(14) Ho, R.Y. N.; Roelfes, G.; Hermant, R.; Hage, R.; Feringa, B. L.; Que, L. Jr. *Chem. Commun.* **1999**, 2161−2162. (b) Ho, R.Y. N.; Roelfes, G.; Feringa, B. L.; Que, L. Jr. *J. Am. Chem. Soc.* **1999**, *121*, 264−265.

(15) Sawyer, D. T. In *Oxygen Chemistry*; Sawyer, D. T., Ed.; Oxford University Press: New York, 1991; Ch. 6.

(16) Klopstra, M.; Roelfes, G.; Hage, R.; Kellogg, R. M.; Feringa, B. L. *Eur. J. Inorg. Chem.* **2004**, 846−856.

(17) de Boer, J. W.; Browne, W. R.; Brinksma, J.; Alsters, P. L.; Hage, R.; Feringa, B. L. *Inorg. Chem.* **2007**, *46*, 6353−6372.

(18) Nanthakumar, A.; Fox, S.; Murthy, N. N.; Karlin, K. D. *J. Am. Chem. Soc.* **1997**, *119*, 3898−3906.

(19) (a) König, E.; Watson, K. J. *Chem. Phys. Lett.* **1970**, *6*, 457−459. (b) Matouzenko1, G. S.; Létard, J. F.; Lecocq, S.; Bousseksou, A.; Capes, L.; Salmon, L.; Perrin, M.; Kahn, O.; Collet, A. *Eur. J. Inorg. Chem.* **2001**, *11*, 2935−2945.

(20) Posse, G. M. E.; Juri, M. A.; Aymonino, P. J.; Piro, O. E.; Negri, H. A.; Castellano, E. E. *Inorg. Chem.* **1984**, *23*, 948−952.

(21) Zang, Y.; Kim, J.; Dong, Y.; Wilkinson, E. C.; Appelman, E. H.; Que, L. Jr. *J. Am. Chem. Soc.* **1997**, *119*, 4197−4205.

(22) (a) Soo, H. S.; Komor, A. C.; Iavarone, A. T.; Chang, C. J. *Inorg. Chem.* **2009**, *48*, 10024−10035. (b) Campanali, A. A.; Kwiecien, T. D.; Hryhorczuk, L.; Kodanko, J. J. *Inorg. Chem.* **2010**, *49*, 4759−4761.

(23) Wolf, M. M. N.; Gross, R.; Schumann, C.; Wolny, J. A.; Schunemann, V.; Dossing, A.; Paulsen, H.; McGarvey, J. J.; Diller, R. *Phys. Chem. Chem. Phys.* **2008**, *10*, 4264−4273.

(24) For both **1** and **4** the absorption spectra are unaffected by addition of NaCl (to 0.1 M) indicating that coordination of chloride to the iron(II) complex does not occur in aqueous solution.

(25) Schenker, S.; Stein, P. C.; Wolny, J. A.; Brady, C.; McGarvey, J. J.; Toftlund, H.; Hauser, A. *Inorg. Chem.* **2001**, *40*, 134−139.

(26) A titration of an aqueous solutions of **1** is shown in Figure S14 where conversion to the parent acetonitrile bound complex is observed to reach a limit at a concn. of 50 mM (with respect to **1**) acetonitrile.

(27) (a) Spiro, T. G.; Czernuszewicz, R. S. Resonance Raman Spectroscopy. In *Physical Methods in Bioinorganic Chemistry*; Que, L., Jr., Ed.; University Science Books: Sausalito, CA, 2000; Ch. 2, pp 59−120. (b) Browne, W. R.; McGarvey, J. J. *Coord. Chem. Rev.* **2007**, *251*, 454−473.

(28) Hirakawa, A. Y.; Tsuboi, M. *Science* **1975**, *188*, 359−361.

(29) McClanahan, S.; Kincaid, J. *J. Raman Spectrosc.* **1984**, *15*, 173−178.

(30) Brady, C.; Callaghan, P. L.; Ciunik, Z.; Coates, C. G.; Dossing, A.; Hazell, A.; McGarvey, J. J.; Schenker, S.; Toftlund, H.; Trautwein, A. X.; Winkler, H.; Wolny, J. A. *Inorg. Chem.* **2004**, *43*, 4289−4299.

(31) Basu, A.; Gafney, H. D.; Strekas, T. C. *Inorg. Chem.* **1982**, *21*, 2231−2235.

(32) It should be noted that the ligand exchange with H_2O is not coupled to the electron transfer process as shown by the increased reversibility at higher scan rates, Figure S34, and hence an EC mechanism is in operation.

(33) Collins, M. J.; Ray, K.; Que, L. Jr. *Inorg. Chem.* **2006**, *45*, 8009–8011.
(34) (a) Fenn, J. B.; Mann, M.; Meng, C. K.; Wong, S. F.; Whitehouse, C. M. *Mass Spectrom. Rev.* **1990**, *9*, 37–70. (b) Kim, J. H.; Dong, Y. H.; Larka, E.; Que, L. *Inorg. Chem.* **1996**, *35*, 2369–2372. (c) Feichtinger, D.; Plattner, D. *Angew. Chem., Int. Ed. Engl.* **1997**, *36*, 1718–1719. (d) Feichtinger, D.; Plattner, D. *J. Chem. Soc., Perkin Trans.* **2000**, *2*, 1023–1028. (e) Gilbert, B. C.; Smith, J. R. L.; Mairata i Payeras, A.; Oakes, J. *Org. Biomol. Chem.* **2004**, *2*, 1176–1180. (f) Bortolini, O.; Conte, V. *Mass Spectrom. Rev.* **2006**, *25*, 724–740.
(35) Several factors limit the amount of information that can be gained from ESI-MS including the lack of control of pH in the electrospray itself, the requirement for addition of a cosolvent, and the oxidation of the complex by molecular oxygen under the dilute conditions required for mass spectrometry.
(36) The assignment of this m/z with regard to oxidation state (Fe^{II}/Fe^{III}) is uncertain. Campanali and co-workers[23b] have assigned this mass as the $[Fe^{II}(N4Py)(OH_2)]^{2+}$, however the pK_a for this species (as determined by the Pourbaix plot in this study) is 4.5 and hence it is unlikely that at pH 6 (the pH employed in the earlier work) that the protonated complex is present. Hence our assignment of this m/z signal is to the $[Fe^{III}(N4Py)(OH)]^{2+}$species.
(37) The assignment of which pyridine ring detaches made in scheme 2 is based on the expected differences in flexibility of each of the pyridine rings.